Developed turbulence and non-linear amplification of magnetic fields in laboratory and astrophysical plasmas

J. Meinecke[a,1], P. Tzeferacos[b], A. R. Bell[a], R. Bingham[c,d], R. J. Clarke[c], E. M. Churazov[e,f], R. Crowston[g], H. Doyle[a], R. P. Drake[h], R. Heathcote[c], M. Koenig[i], Y. Kuramitsu[j,k], C. C. Kuranz[h], D. Lee[l], M. J. MacDonald[h], C. D. Murphy[g], M. M. Notley[c], H.-S. Park[m], A. Pelka[i,n], A. Ravasio[i], B. Reville[o], Y. Sakawa[k], W. C. Wan[h], N. C. Woolsey[g], R. Yurchak[i], F. Miniati[p], A. A. Schekochihin[a], D. Q. Lamb[b], G. Gregori[a,b,1]

May 5, 2015

[a]Department of Physics, University of Oxford, Parks Road, Oxford OX1 3PU, UK
[b]Department of Astronomy and Astrophysics, University of Chicago, 5640 S. Ellis Ave, Chicago, IL 60637, USA
[c]Rutherford Appleton Laboratory, Chilton, Didcot OX11 0QX, UK
[d]Department of Physics, University of Strathclyde, Glasgow G4 0NG, UK
[e]Max Planck Institute for Astrophysics, Karl-Schwarzschild-Strasse 1, D-85741 Garching, Germany
[f]Space Research Institute (IKI), Profsouznaya 84/32, Moscow, 117997, Russia
[g]Department of Physics, University of York, Heslington, York, YO10 5D, UK
[h]Atmospheric, Oceanic, Space Science, University of Michigan, 2455 Hayward St, Ann Arbor, MI 48109, USA
[i]Laboratoire pour l'Utilisation de Lasers Intenses, UMR7605, CNRS CEA, Université Paris VI Ecole Polytechnique, 91128 Palaiseau Cedex, France
[j]Department of Physics, National Central University, No. 300, Jhongda Rd., Jhongli, Taoyuan, 320 Taiwan
[k]Institute of Laser Engineering, Osaka University, 2-6 Yamadaoka, Suita, Osaka 565-0871, Japan
[l]Applied Mathematics and Statistics, University of California, Santa Cruz, CA 96064, USA
[m]Lawrence Livermore National Laboratory, Livermore, CA 94550, USA
[n] Institute of Radiation Physics, Helmholtz-Zentrum Dresden-Rossendorf, Germany
[o]School of Mathematics and Physics, Queens University Belfast, Belfast BT7 1NN, UK

[p]Department of Physics, ETH Zürich, Wolfgang-Pauli-Strasse 27, CH-8093 Zürich, Switzerland

[1]To whom correspondence should be addressed; E-mail: jena.meinecke@physics.ox.ac.uk; g.gregori1@physics.ox.ac.uk.

The visible matter in the Universe is turbulent and magnetized: turbulence in galaxy clusters is produced by mergers and by jets of the central galaxies and believed responsible for the amplification of magnetic fields. We report on experiments looking at the collision of two laser-produced plasma clouds, mimicking in the laboratory a cluster merger event. By measuring the spectrum of the density fluctuations, we infer developed, Kolmogorov-like turbulence. From spectral line broadening, we estimate a level of turbulence consistent with turbulent heating balancing radiative cooling, as it likely does in galaxy clusters. We show that the magnetic field is amplified by turbulent motions, reaching a nonlinear regime that is a precursor to turbulent dynamo. Thus, our experiment provides a promising platform for understanding the structure of turbulence and the amplification of magnetic fields in the Universe.

Keywords: Turbulence, Galaxy clusters, Magnetic field amplification

Significance statement

Magnetic fields exist throughout the Universe. Their energy density is comparable to the energy density of the fluid motions of the plasma in which they are embedded, making magnetic fields essential players in the dynamics of the luminous matter in the Universe. The origin and the amplification of these magnetic fields to their observed strengths are far from being understood. The standard model for the origin of these galactic and intergalactic magnetic fields is through the amplification of seed fields via turbulent processes to the level consistent with current observations. For this process to be effective the amplification needs to reach a strongly non-linear phase. Experimental evidence of the initial non-linear amplification of magnetic fields is presented in this paper.

In the early universe, matter was nearly homogenously distributed; today, as a result of gravitational instabilities, it forms a web-like structure consisting of filaments and galaxy clusters [1]. The continued mergers of galaxies, filaments, and galaxy clusters inject turbulence into the intergalactic medium via shocks [2, 3]. At the same time, the existence of diffuse synchrotron emission at radio wavelengths and Faraday rotation measurements indicate the presence of magnetic fields in galaxy clusters with strengths up to tens of μG [4, 5]. The standard model for the origin of these intergalactic magnetic fields is amplification of seed fields via the turbulent dynamo mechanism to the present-day observed values [6, 7, 8, 9, 10], but other possibilities involving plasma kinetic instabilities [11, 12, 13, 14], return currents [15, 16] or primordial mechanisms [17, 18] have also been invoked.

We have carried out experiments involving the collision of two plasma jets – reminiscent of cluster merger events – to produce a laboratory-scale replica of a turbulent intracluster plasma, although obviously our plasma is not confined in a dark matter potential well, as it is in clusters. In the intracluster medium, large-scale turbulent motions are influenced by density stratification and gravity. However, at smaller spatial scales the time periods for buoyancy-driven motions are much longer than those of the turbulent motions, so the fluctuations at these scales are universal, and thus similar to the turbulence we can create in our laboratory experiments The scale invariance of hydrodynamic equations [19, 20] implies, if we assume that a distance of 1 cm in the laboratory corresponds to 100 kpc in the astrophysical case, that 1 μs becomes 0.5 Gyr and a density of 4×10^{17} cm^{-3} is equivalent to 0.01 cm^{-3} in the galaxy cluster.

Our experiments were conducted using the Vulcan laser of the Central Laser Facility at the Rutherford Appleton Laboratory. We have focussed multiple laser beams (with $\sim$240 J total energy and $\sim$1 ns pulse duration) onto a carbon foil to launch a plasma jet into an ambient argon gas-filled chamber (at a pressure of 1 mbar). A full description of the experimental set-up is given in Fig. 1. Ablation of target material by the laser drives a shock into the carbon

foil, which then produces a collimated jet from the back surface of the target (i.e., the side opposite to that illuminated by the laser). The target material ablated by the laser is slowed by the ambient medium, creating a wrap-around shock, visible in Fig. 1. Schlieren measurements were taken to characterize the outflows at various times. The fastest moving material occurs on axis (see Fig. 2) with $v_0 \sim 25$ km/s ($v_0/c_s \sim 4$, where c_s is the sound speed) at 3 cm from the target, while material on the edges of the jet moves more slowly as a result of Kelvin-Helmholtz shearing instabilities. Experiments were also performed using two sets of laser beams, each set illuminating a carbon foil, producing two jets that collide. The collision drives strong turbulence in a region that grows from a size $L \sim 1$ cm at $t = 0.8$ μs to ~ 2 cm at $t > 1.5$ μs, at which time the turbulence reaches a more relaxed state.

The turbulent velocity fluctuations on the system scale L can be estimated from Fig. 2b. At the collision point, the observed argon emission lines are broadened by ∼0.2 nm. Half of this broadening is attributed to the increased density, and to a lesser extent to the higher temperatures (thermal broadening is small due to the large ion mass) – see supplementary material. The broadening due to turbulent motions is then ∼0.1 nm, corresponding to a turbulent velocity $v_{\rm turb} \approx 27 \pm 5$ km/s. Thus, $v_{\rm turb} \sim v_0$, suggesting that the collision effectively randomizes the directed velocities of the two jets. Taking the measured values of jet velocity, density, and temperature in the collision region, and assuming an ionization state $Z \sim 2.5$ for argon, we estimate the inter-jet electron-ion ($\lambda_{ei} \approx 0.04$ cm) and ion-ion ($\lambda_{ii} \approx 0.005$ cm) mean free paths to be significantly smaller than the size of the jets. This confirms that the two jets strongly interact via Coulomb collisions and the contact surface between the two jets becomes quickly unstable. The Reynolds number calculated with respect to the scale L is thus ${\rm Re} = v_{\rm turb} L/\nu \sim 1.0 \times 10^6$ ($\nu \approx 2.8$ cm^2/s is the kinematic viscosity of the plasma).

For our plasma conditions the radiative cooling rate per ion is $Q_{\rm cool} \sim m_{\rm ion} \kappa_P \sigma_{SB} T^4 \sim 0.5$ eV/ns, where $m_{\rm ion}$ is the argon mass, $\kappa_P \sim 8 \times 10^4$ cm^2/g is the Planck opacity (see sup-

plementary information), and σ_{SB} is the Stefan-Boltzmann constant. This implies that during one jet crossing time, $\sim L/v_0 \approx 400$ ns, the plasma should have cooled to near 1 eV, as in the case of a single jet expansion (detailed calculations are provided in the supplementary information). Fig. 2 instead shows that in the collision region the temperature remains $\gtrsim$2 eV over a few L/v_0, suggesting that much of the cooling must be offset by heating. Turbulent motions are eventually dissipated into heat. This heating rate per ion can be approximated to be $Q_{\rm turb} \sim m_{\rm ion} v_{\rm turb}^3/L \sim 0.6$ eV/ns. Thus $Q_{\rm turb} \sim Q_{\rm cool}$, consistent with turbulence playing an important role in achieving a stable temperature profile, with near balance between turbulent heating and radiative cooling.

We performed simulations of the experiments using the FLASH code [21, 22] (see supplementary material). The results of the FLASH simulations are consistent with the measured properties of the jet, including its morphology and the physical conditions in the interaction region (Figs. 1 and 2). The simulations indicate enhanced vorticity as the two jets collide, and reproduce the increase in the electron density and the moderate rise in the temperature after the collision.

In some respects, our experimental conditions are qualitatively similar to those found in galaxy cluster, where heating driven by turbulent motions in the intracluster plasma reduces radiative losses and decreases the net cooling rate [23]. On the other hand, while in the inertial range energy is transferred from one scale to another at a rate given by $Q_{\rm turb}$, which has the same form both in clusters and laboratory experiments, the actual mechanism for energy dissipation into heat can be different. This is dominated by collisional, isotropic viscosity in the laboratory, whereas in clusters, at a minimum, one must take into account that viscosity is anisotropised due to magnetic fields and furthermore kinetic processes may play an important role [8]. Thus the similarity between the laboratory "replica" and the astrophysical reality can only hold at scales larger than the viscous one.

During hierarchical structure formation, clusters form from accretion of filaments, galaxies, galaxy groups, and cluster mergers. In clusters of galaxies, turbulent velocities can be inferred from the density perturbations, which, in turn, are obtained using the measured X-ray radiation intensities [23, 24, 25]. The turbulence in clusters is mainly sub-sonic at small scales (and near sonic at large scales), so density fluctuations (injected at large scales) behave like a passive scalar. Therefore the density and velocity spectra are expected to be the same [26]. The fact that turbulence is moderately supersonic in our experiment while sub-sonic in clusters, is likely to lead to only a a modest change in the power spectra (and at small enough scales, motions will in any event become sub-sonic). Indeed, spectroscopic observations of supersonic motions in molecular clouds [27] suggest a velocity power spectrum close to the classical Kolmogorov $k^{-5/3}$ law (where k is the wavenumber) that holds for incompressible fluids. Numerical simulations of supersonic turbulence show a spectrum somewhat steeper than Kolmogorov's, $k^{-1.7}$ to k^{-2}, depending on the details of the driving mechanism [28]. These differences are smaller that the uncertainties in our power spectrum measurements.

We have extracted the power spectrum of the electron density fluctuations from our data. The result is shown in Fig. 3a, using the wavelet method discussed in Ref. [25], which was used there for the analysis of X-ray maps of the Coma cluster. The spectrum is consistent with a Kolmogorov-like power law as expected from the theoretical work we discuss above, suggesting that we do indeed see fully developed turbulence. A similar spectrum was obtained in galaxy clusters [24, 25].

While $\mathrm{Re} \gg 1$ and turbulent motions are excited over a large range of scales, the magnetic Reynolds number is $\mathrm{Rm} = v_{\mathrm{turb}} L/\eta \sim 14$ ($\eta = 1.9 \times 10^5$ cm^2/s is the resistivity), so the resistive scale lies well above the viscous scale, and close to the system scale, L. Since Rm is not very large in the experiment, the full magneto-hydrodynamic (MHD) scaling between the cluster and the laboratory is only marginally valid [20]. At such Rm, turbulent dynamo,

believed to be the mechanism whereby strong fields are generated in galaxy clusters [8, 7], does not operate, but the magnetic fields can be amplified via stochastic tangling of an imposed field by turbulent motions [29, 30]. At small Rm ($\lesssim 1$), the amplified field grows proportionally to Rm and has the Golitsyn [29] $k^{-11/3}$ power law, which arises in Kolmogorov turbulence when the stochastic tangling of the magnetic field is balanced by Ohmic diffusion. As Rm gets larger the scaling of the amplified field gets closer to $\mathrm{Rm}^{1/2}$, and its spectrum becomes shallower [31]. Eventually, there is a transition to the turbulent dynamo regime, expected at Rm~ 200.

In our experiment, magnetic fields are generated before the collision via the Biermann battery mechanism [32, 33], which is sustained by the shearing instability between the jet and the ambient medium. It is this field that is then tangled and amplified by turbulent motions. Fig. 4 shows that the magnetic field is larger by a factor $\sim$2-3 in the case of collision of the two jets compared to the unperturbed single jet. The FLASH simulation reproduces the morphology and time behavior of the magnetic field, including the time at which the field changes sign. We expect the simulation to underpredict the peak magnetic field in the colliding jets case since turbulent amplification is not properly captured in 2D geometry.

Most importantly, the amplified magnetic field detected in the experiment is larger than the Biermann battery produced field. This suggests that amplification has reached the non-linear regime, with the amplified field roughly proportional to $\mathrm{Rm}^{1/2}$. This conclusion is further supported by measurement of the magnetic energy spectrum $M(\omega)$, shown in Fig. 3b. Translated into wavenumber spectrum, this spectrum is $M(k) \sim k^{-17/9}$ (see the supplementary material), substantially shallower than the low-Rm Golitsyn spectrum $k^{-11/3}$ [29], which we observe in the case of no jet collision, so both less turbulence and lower Rm [10]. The emergence of progressively shallower magnetic spectra is a sign of nonlinear field amplification, which is a precursor to turbulent dynamo [31].

Despite important differences, the laboratory simulation of an intracluster plasma that we

have created offers a new tool for modelling the amplification of magnetic fields by turbulent astrophysical plasmas.

References and Notes

[1] Miniati F, et al. (2000) Properties of cosmic shock waves in large-scale structure formation. *Astrophys. J.* 542:608–621.

[2] Norman ML, Bryan GL (1999) *Cluster Turbulence*, Lecture Notes in Physics, Berlin Springer Verlag eds Röser HJ, Meisenheimer K Vol. 530, p 106.

[3] Miniati F (2014) the Matryoshka Run: a Eulerian Refinement Strategy To Study the Statistics of Turbulence in Virialized Cosmic Structures. *Astrophys. J.* 782:21.

[4] Govoni F, Feretti L (2004) Magnetic fields in clusters of galaxies. *Int J Mod Phys D* 13:1549–1594.

[5] Bernet ML, Miniati F, Lilly SJ, Kronberg PP, Dessauges Zavadsky M (2008) Strong magnetic fields in normal galaxies at high redshift. *Nature* 454:302–304.

[6] Parker EN (1955) Hydromagnetic Dynamo Models. *Astrophys. J.* 122:293–314.

[7] Zweibel EG, Heiles C (1997) Magnetic fields in galaxies and beyond. *Nature* 385:131–136.

[8] Schekochihin AA, Cowley SC (2006) Turbulence, magnetic fields, and plasma physics in clusters of galaxies. *Phys. Plasmas* 13:056501.

[9] Ryu D, Kang H, Cho J, Das S (2008) Turbulence and Magnetic Fields in the Large-Scale Structure of the Universe. *Science* 320:909–912.

[10] Meinecke J, et al. (2014) Turbulent amplification of magnetic fields in laboratory laser-produced shock waves. *Nature Phys.* 10:520–524.

[11] Schlickeiser R, Shukla PK (2003) Cosmological Magnetic Field Generation by the Weibel Instability. *Astrophys. J.* 599:L57–L60.

[12] Medvedev MV, Silva LO, Kamionkowski M (2006) Cluster Magnetic Fields from Large-Scale Structure and Galaxy Cluster Shocks. *Astrophys. J.* 642:L1–L4.

[13] Huntington CM, et al. (2015) Observation of magnetic field generation via the weibel instability in interpenetrating plasma flows. *Nature Physics* 11:173–176.

[14] Park HS, et al. (2015) Collisionless shock experiments with lasers and observation of weibel instabilities. *Phys. Plasmas* In press.

[15] Langer M, Aghanim N, Puget J (2005) Magnetic fields from reionisation. *Astron. Astrophys.* 443:367–372.

[16] Miniati F, Bell AR (2011) Resistive magnetic fields at cosmic dawn. *Astrophys. J.* 729:73.

[17] Harrison ER (1970) Generation of magnetic fields in the radiation era. *Mon. Not. R. Astron. Soc.* 147:279–286.

[18] Durrer R, Neronov A (2013) Cosmological magnetic fields: their generation, evolution and observation. *Astron Astrophys Rev* 21:62.

[19] Ryutov D, et al. (1999) Similarity Criteria for the Laboratory Simulation of Supernova Hydrodynamics. *Astrophys. J.* 518:821–832.

[20] Cross JE, Reville B, Gregori G (2014) Scaling of magneto-quantum-radiative hydrodynamic equations: from laser-produced plasmas to astrophysics. *Astrophys. J.* 795:59.

[21] Tzeferacos P, et al. (2012) Magnetohydrodynamic simulations of shock-generated magnetic field experiments. *High Energy Dens. Phys.* 8:322–328.

[22] Tzeferacos P, et al. (2014) Flash mhd simulations of experiments that study shock-generated magnetic fields. *High Energy Dens. Phys.* in press.

[23] Zhuravleva I, et al. (2014) Turbulent heating in the x-ray brightest galaxy clusters. *Nature* 515:85–87.

[24] Schuecker P, Finoguenov A, Miniati F, Böhringer H, Briel U (2004) Probing turbulence in the Coma galaxy cluster. *Astron. Astrophys.* 426:387–397.

[25] Churazov E, et al. (2012) X-ray surface brightness and gas density fluctuations in the Coma cluster. *Mon. Not. R. Astron. Soc.* 421:1123–1135.

[26] Zhuravleva I, et al. (2014) the Relation Between Gas Density and Velocity Power Spectra in Galaxy Clusters: Qualitative Treatment and Cosmological Simulations. *Astrophys. J.* 788:L13.

[27] Larson RB (1981) Turbulence and star formation in molecular clouds. *Mon. Not. R. Astron. Soc.* 194:809–826.

[28] Federrath C (2013) On the universality of supersonic turbulence. *Mon. Not. R. Astron. Soc.* 436:1245–1257.

[29] Golitsyn GS (1960) Fluctuations of the Magnetic Field and Current Density in a Turbulent Flow of a Weakly Conducting Fluid. *Soviet Phys. Doklady* 5:536–539.

[30] Moffatt HK (1961) The amplification of a weak applied magnetic field by turbulence in fluids of moderate conductivity. *J. Fluid Mech.* 11:625–635.

[31] Schekochihin AA, et al. (2007) Fluctuation dynamo and turbulent induction at low magnetic Prandtl numbers. *New J. Phys.* 9:300.

[32] Biermann L (1950) Über den Ursprung der Magnetfelder auf Sternen und im interstellaren Raum. *Z. Naturforsch. A* 5:65–71.

[33] Gregori G, et al. (2012) Generation of scaled protogalactic seed magnetic fields in laser-produced shock waves. *Nature* 481:480–483.

[34] MacFarlane J, I. Golovkin, Wang P, Woodruff P, Pereyra N (2007) Spect3d – a multi-dimensional collisional-radiative code for generating diagnostic signatures based on hydrodynamics and PIC simulation output. *High Energy Dens. Phys.* 3:181–190.

[35] Settles GS (2001) *Schlieren and Shadowgraph Techniques* (Springer).

[36] Fryxell B, et al. (2000) FLASH: An Adaptive Mesh Hydrodynamics Code for Modeling Astrophysical Thermonuclear Flashes. *Astrophys. J.* 131:S273–S334.

[37] Dubey A, et al. (2009) Extensible component-based architecture for FLASH, a massively parallel, multiphysics simulation code. *Parall. Comp.* 35:512–522.

[38] Lee D (2013) A solution accurate, efficient and stable unsplit staggered mesh scheme for three dimensional magnetohydrodynamics. *J. Comp. Phys.* 243:269–292.

[39] Fatenejad M, et al. (2013) Modeling HEDLA magnetic field generation experiments on laser facilities. *High Energy Dens. Phys.* 9:172–177.

[40] Li S (2005) An HLLC Riemann solver for magneto-hydrodynamics. *J. Comp. Phys.* 203:344–357.

[41] Kerley S (1972) Equation of state and phase diagram of dense hydrogen. *Phys. Earth Planet. Inter.* 6:78–82.

[42] Y. B. Zel'dovich and Y. P. Raizer (1966) *Physics of shock waves and high temperature hydrodynamic phenomena* (Academic).

[43] MacFarlane J, I. Golovkin, Woodruff P (2006) HELIOS-CR – A 1-D radiation-magnetohydrodynamics code with inline atomic kinetics modeling. *J. Quant. Spect. Radiat. Transfer* 99:381–397.

[44] R. W. P. McWhirter (1978) Review paper A5. Data needs, priorities and accuracies for plasma spectroscopy. *Phys. Rep.* 37:165–209.

[45] G. D. Tsakiris and K. Eidmann (1987) An approximate method for calculating Planck and Rosseland mean opacities in hot, dense plasmas. *J. Quant. Spect. Radiat. Transfer* 8:353–368.

[46] A. Malagoli, R. Rosner and G. Bodo (1987) On the thermal instability of galactic and cluster halos. *Astrophys. J.* 319:632–636.

[47] G. I. Taylor (1938) The Spectrum of Turbulence. *Proc. R. Soc. Lond. A* 164:467–490.

[48] H.-S. Park *et al.* (2012) Studying astrophysical collisionless shocks with counterstreaming plasmas from high power lasers. *High Energy Dens. Phys.* 8:38–45.

[49] R. P. Drake and G. Gregori (2012) Design Considerations for Unmagnetized Collisionless-Shock Measurements in Homologous Flows. *Astrophys. J.* 479:171.

[50] T. N. Kato and H. Takabe (2008) Nonrelativistic Collisionless Shocks in Unmagnetized Electron-Ion Plasmas. *Astrophys. J.* 681:L93–L96.

[51] S. Ichimaru (2004) *Statistical plasma physics* (Westview).

Acknowledgements

We thank the Vulcan technical team at the Central Laser Facility of the Rutherford Appleton Laboratory for their support during the experiments. The research leading to these results has received funding from the European Research Council under the European Community's Seventh Framework Programme (FP7/2007-2013) / ERC grant agreements no. 256973 and 247039, and the U.S. Department of Energy under Contract No. B591485 to Lawrence Livermore National Laboratory and Field Work Proposal No. 57789 to Argonne National Laboratory. This work was supported in part by NIH through resources provided by the Computation Institute and the Biological Sciences Division of the University of Chicago and Argonne National Laboratory, under grant S10 RR029030-01. Partial support from the Science and Technology Facilities Council and the Engineering and Physical Sciences Research Council of the United Kingdom (Grant No. EP/G007187/1) is also acknowledged. The work of R.P.D, C.C.K., M.J.M., and W.C.W was supported by the USDOE under grant DE-NA0001840.

Author Contributions

G. G., D. Q. L, A. A. S., B. R. and F. M. conceived this project, and it was designed by G. G., J. M., B. R., C. D. M., R. B., A. A. S., N. C. W., and R. P. D. The Vulcan experiment was carried out by J. M., H. W. D., M. J. M., R. C., C. K., C. D. M., A. P., W. C. W, R. J. C, R. H., and M. M. N. The paper was written by J. M., G. G., H. W. D., A. A. S., A. R. B., D. Q. L., P. T. and B. R. The data was analyzed by J. M., H. W. D., and E. C. Numerical simulations were performed by P. T. Further experimental and theoretical support was provided by A. R. B., M. F., M. K., Y. K., D. Q. L., D. L., H.-S. P., A. R., B. A. R., Y. S., A. S., P. T., N. C. W., and R. Y.

The authors declare no conflict of interest.

Figure Legends

Figure 1: **Colliding jet configuration for the generation of turbulence.** Two carbon foils (100 μm thick, with density 1.13 g/cm^3) are separated by 60 mm in a 1 ± 0.2 mbar argon gas-filled chamber. Each target is ablated by three frequency doubled (527 nm wavelength) laser beams with a laser spot diameter of 300 μm. The total laser illumination onto each foil is 240 ± 30 J in a 1 ns pulse length. An induction coil ($\gtrsim$200 MHz bandwidth, with four twisted pair coils wound around the axis of a $\sim 1 \times 1$ mm^2 plastic core) is placed at equal distance between the foil targets. Additional details are given in Ref. [10]. (a) Schlieren image (using a 532 nm wavelength probe and 5 ns CCD gate width) of the jet formations at $t = 500$ ns after the laser shot. (b) The jets collide at $t = 800$ ns, and (c) turbulence develops by $t = 1500$ ns. (d) Magnetic field (top) and mass density (bottom) from a FLASH simulation of the two jets at $t = 500$ ns. (e) Same as (d) but at $t = 800$ ns. (f) same as (d) but at $t = 1500$ ns. (g) Schlieren synthetic image obtained by post-processing the FLASH results at $t = 500$ ns using Spect3D [34]. (h) Same as (g) but at $t = 800$ ns. (i) same as (g) but at $t = 1500$ ns. The measured and simulated Schlieren images are similar at $t = 500$ and 800 ns, but differ at $t = 1500$ ns. The difference is likely due to a slight angle between the directions the two jets are moving, which allows part of the jets to continue beyond the initial interaction region. This produces a much larger turbulent region in the experiment than in the simulation, where the 2D cylindrical geometry prevents us from accommodating this situation. Since the FLASH simulations are 2D cylindrical, the plane that most closely corresponds to the experimental data is the one that is perpendicular to the page and connects the two target foils. This plane does not contain the induction coil probe.

Figure 2: **Characterization of jet propagation and collision.** (a) Measurement of the jet leading edge *vs* time from Schlieren data (blue symbols) and FLASH simulations (dashed green line). The FLASH simulation was calibrated to match the position of the leading edge of the jet at 800 ns for the measured value of the total laser energy for that data point. The inset shows the electron density profile obtained by interferometry at $t = 800$ ns compared to FLASH predictions. The density has been averaged over a volume of 5 mm radius from the axis connecting the two target foils. (b) Spatially resolved electron temperature profile of a single jet (blue symbols) and colliding jets (red symbols) at $t = 800$ ns obtained from the measured argon spectral lines (see supplementary information for details). Solid lines (blue: single jet; and, red: colliding jets) correspond to the predicted temperature values from FLASH simulations at $t = 800$ ns, averaged over the same volume as the electron density. Dashed lines are the results from the same FLASH simulations at $t = 1500$ ns. The inset shows an example of the argon spectral line at $t = 800$ ns and 3 cm from the carbon foil target (averaged over 0.1 cm).

Figure 3: **Power spectra of turbulence**. (a) Plot of the density fluctuation power spectrum $P(k) = |n_k/n_0|^2$, where n_k is the discrete Fourier transform of the space-dependent electron density and n_0 its average value. In Schlieren imaging, the measured signal intensity is proportional to $\int(\partial n/\partial y + \partial n/\partial z)dx$, where n is the electron density, x,y are the image-plane spatial co-ordinates and z the depth [35]. Therefore, under the assumption that turbulence is statistically homogeneous across the jet interaction region, the discrete Fourier transform of the central region of the jet collision in Fig. 1c directly gives n_k. The power spectrum is arbitrarily normalized so that $P(k) \approx 1$ at the largest scale. The solid red curve corresponds to the experimental data, while the black and green symbols correspond to the inferred density spectrum in the Coma cluster obtained from CHANDRA and XMM satellite observations, respectively [25]. (b) Plot of the magnetic energy spectrum $M(\omega) = |B(\omega)|^2$, where $B(\omega)$ is the discrete Fourier transform of the total magnetic field for both the cases with a single jet (red solid line) and with colliding jets (blue solid line). The slope of the spectrum in the case of colliding jets is shallower than in the case of a single jet (where it is consistent with the $k^{-11/3}$ Golitsyn spectrum, assuming conversion from frequencies to wave numbers according to Taylor hypothesis, $\omega \sim v_0 k$). This gradual shallowing of the spectrum with increasing Rm is a signature of the dynamo precursor regime [31]. The measured frequency spectrum $\sim\omega^{-7/3}$ can be argued to correspond to wavenumber spectrum $\sim k^{-1.9}$ in the case of colliding jets, where Taylor hypothesis is inapplicable (see supplementary information).

Figure 4: **Time evolution of the magnetic field.** (a) The magnetic field components measured at 3 cm from the carbon foil in the case of a single jet (see Fig. 1 for the axis co-ordinates). (b) Magnetic field components measured in the case of jet collision. The time resolution of the magnetic field traces is 10 ns. These have been extracted from the recorded induction coil voltages. Details are given in Ref. [10]. The initial ($t < 100$ ns) high frequency noise due to the laser-plasma interaction with the target has been filtered. The dashed lines in both panels correspond to the average azimuthal magnetic field obtained from the FLASH simulations in a volume of radius 1 mm and length 3 mm centered at the midpoint between the two target foils. Due to cylindrical symmetry of the simulation domain, the measured component that is closest to the calculated one is B_z.

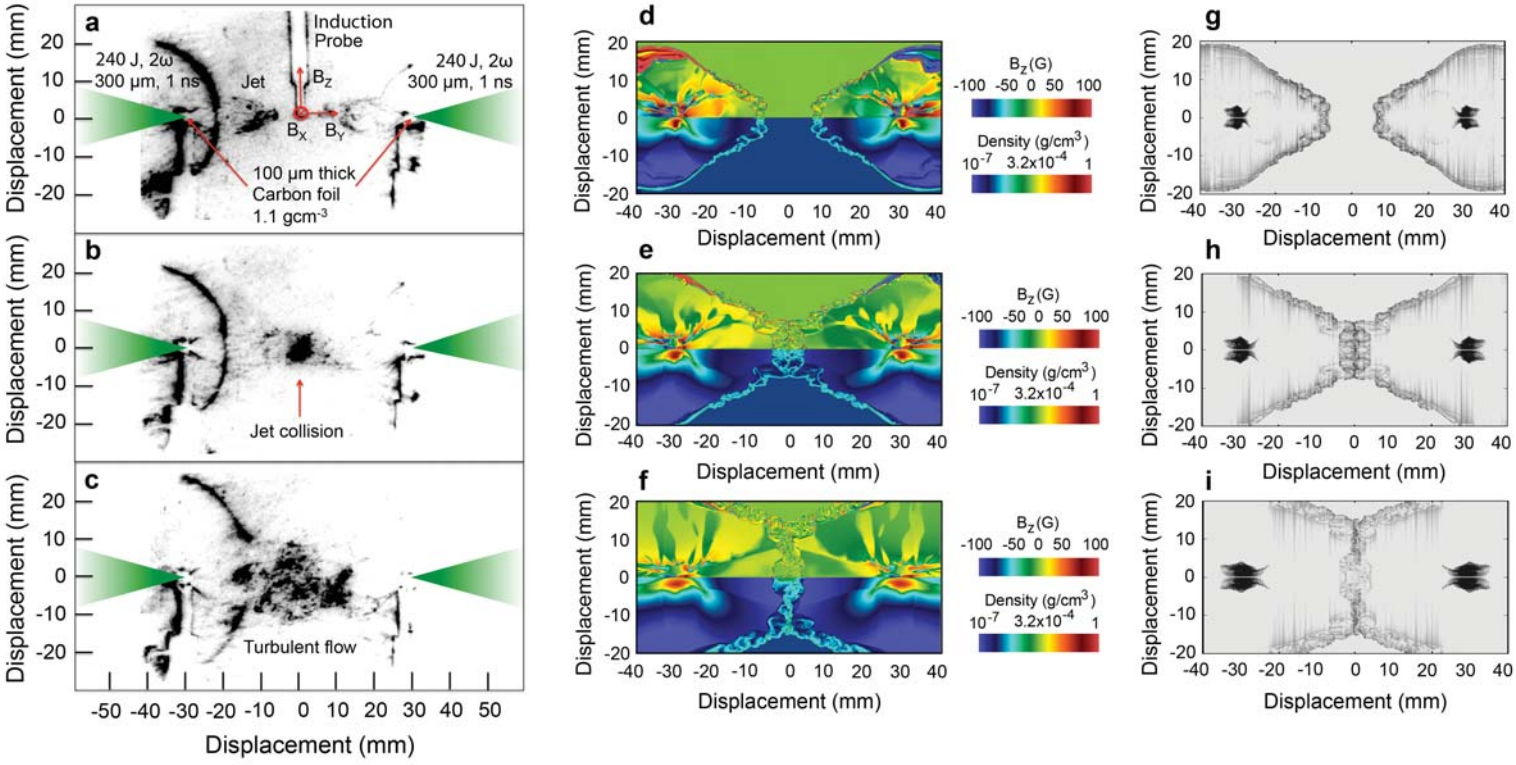
a
Induction
Probe
240 J, 2ω
300 μm, 1 ns
Jet
B_Z
240 J, 2ω
300 μm, 1 ns
B_X
B_Y
100 μm thick
Carbon foil
1.1 gcm^{-3}
b
Jet collision
c
Turbulent flow
Displacement (mm)
Displacement (mm)
d
e
f
B_z(G)
-100 -50 0 50 100
Density (g/cm^3)
10^{-7} $3.2x10^{-4}$ 1
g
h
i

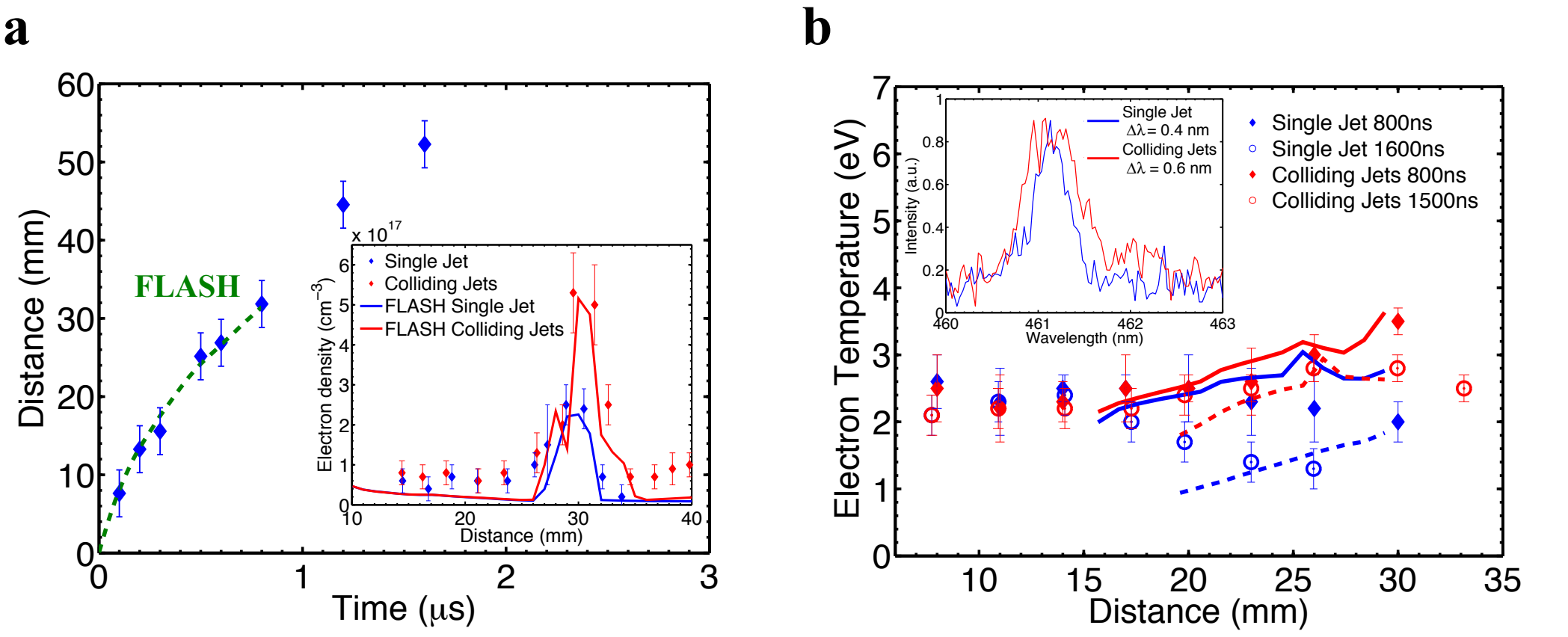
a
Distance (mm)
Time (μs)
FLASH
x 10^17
Electron density (cm^-3)
Single Jet
Colliding Jets
FLASH Single Jet
FLASH Colliding Jets
Distance (mm)
b
Electron Temperature (eV)
Distance (mm)
Single Jet 800ns
Single Jet 1600ns
Colliding Jets 800ns
Colliding Jets 1500ns
Intensity (a.u.)
Single Jet
Δλ= 0.4 nm
Colliding Jets
Δλ = 0.6 nm
Wavelength (nm)

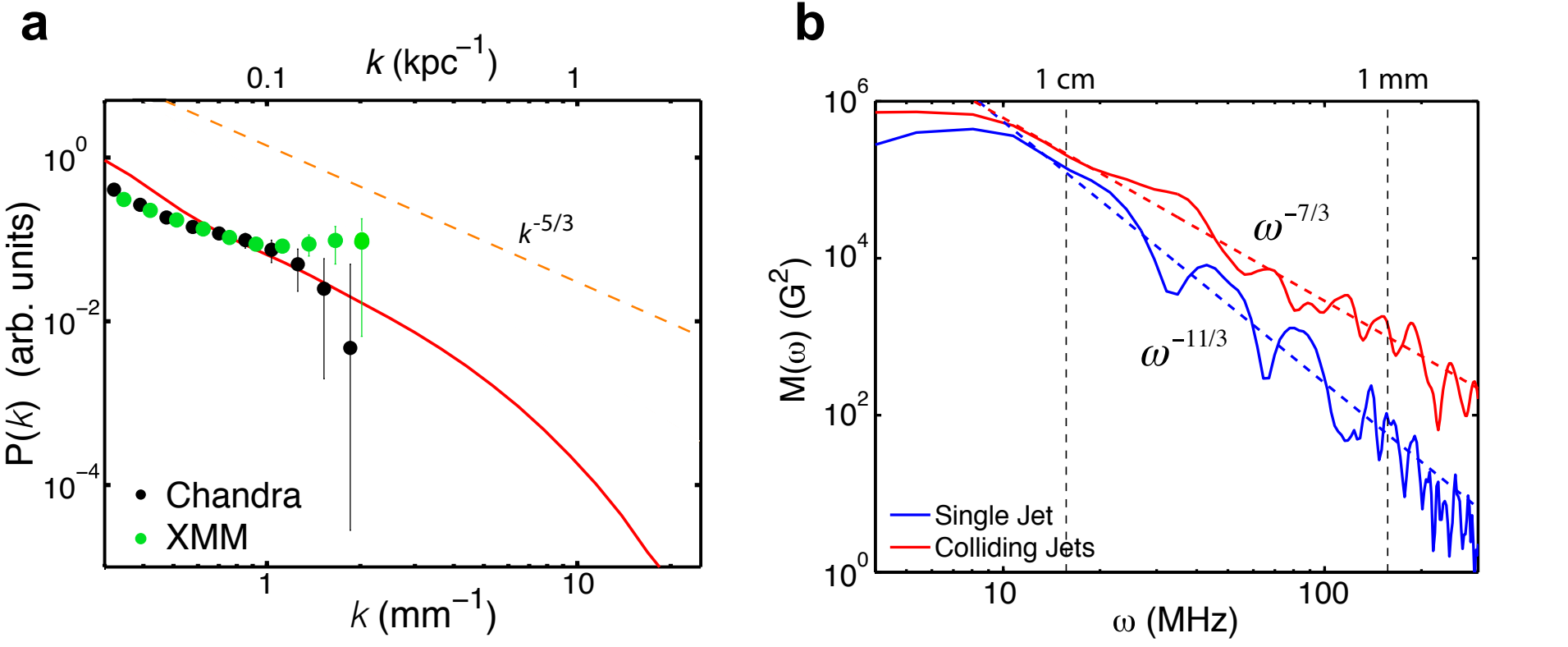
a
0.1
k (kpc−1)
1
10^0
10^−2
10^−4
P(k) (arb. units)
k^-5/3
Chandra
XMM
1
10
k (mm−1)
b
1 cm
1 mm
10^6
10^4
10^2
10^0
M(ω) (G^2)
ω^−7/3
ω^−11/3
Single Jet
Colliding Jets
10
100
ω (MHz)

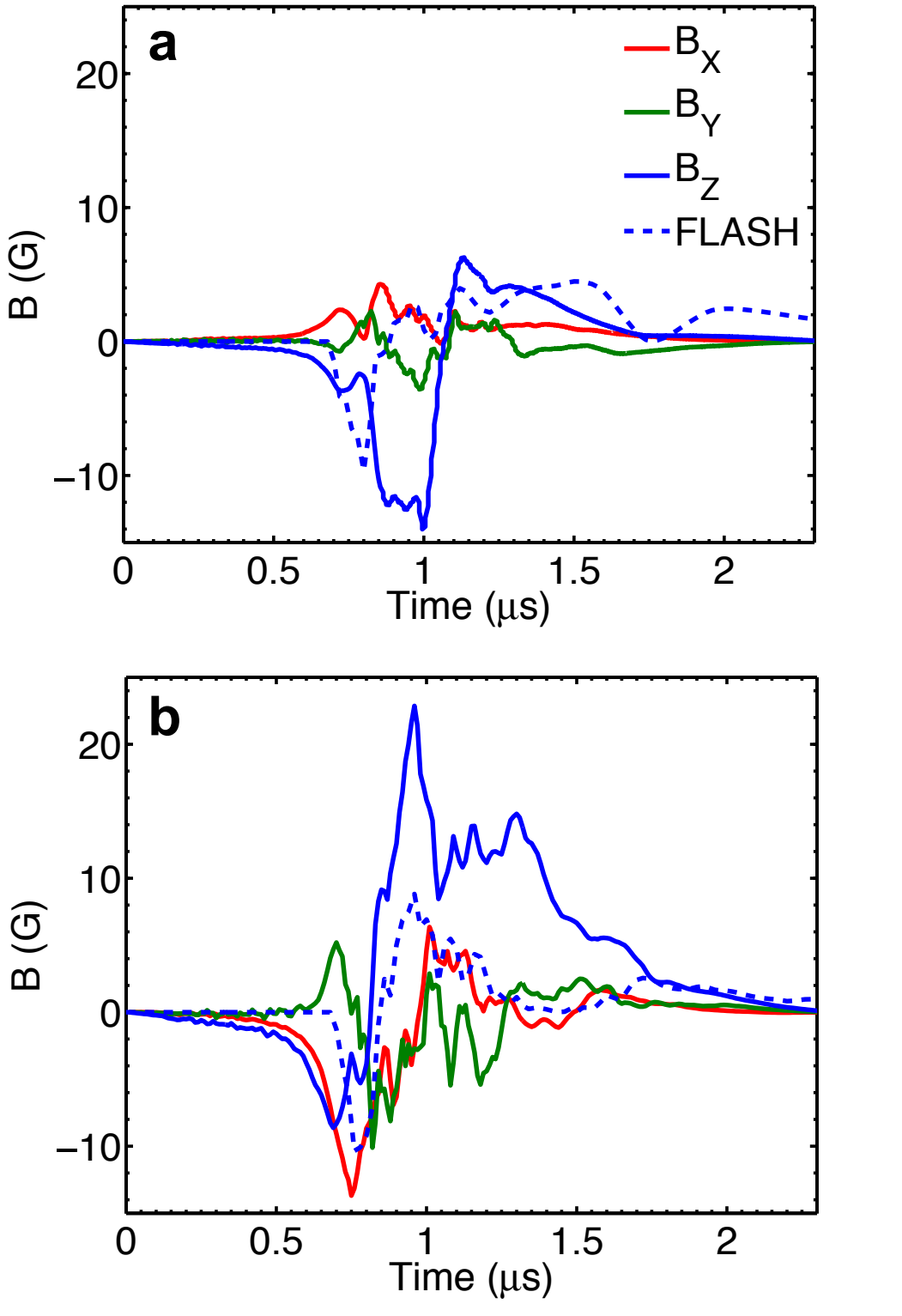
a
B_X
B_Y
B_Z
FLASH
B (G)
20
10
0
−10
0
0.5
1
1.5
2
Time (μs)
b
B (G)
20
10
0
−10
0
0.5
1
1.5
2
Time (μs)